High electrical conductivity in three-dimensional porphyrin-phosphonate metal organic-frameworks

Yunus Zorlu,[1] Patrik Tholen,[2] Mehmet Menaf Ayhan,[1] Ceyda Bayraktar,[1] Gabriel Hanna,[3] A. Ozgur Yazaydin,[4] Özgür Yavuzçetin,[5] Gündoğ Yücesan[2]*

[1]Gebze Technical University, Kimya Bölümü, 41400 Gebze-Kocaeli, Turkey

[2]Technische Universität Berlin, Gustav-Meyer-Allee 25, 13355 Berlin, Germany

[3]University of Alberta, 116 St. and 85 Ave. Edmonton, Alberta T6G 2R3, Canada

[4]University College London, Torrington Place, London WC1E 7JE, United Kingdom

[5] University of Wisconsin-Whitewater, Department of Physics, 800 W. Main St., Whitewater, WI-53190, USA

E-mail: yuecesan@tu-berlin.de

Keywords: metal-organic framework design, electrically conductive metal-organic frameworks, semiconductors, supercapacitors

Herein, we report the design and synthesis of a highly electrically conductive and microporous three-dimensional zinc-phosphonate metal-organic framework [Zn(Cu-*p*-H_4TPPA)] $\cdot 2\,(CH_3)_2NH_2^+$ (designated as GTUB3), constructed using the 5,10,15,20-tetrakis [*p*-phenylphosphonic acid] porphyrin (*p*-H_8TPPA) organic linker. GTUB3 has an indirect band gap of 1.64 eV and a high average electrical conductivity of 4 S/m, making it a rare example of an electrically conductive zinc metal-organic framework. The N_2-accessible geometric surface area of GTUB3, as predicted by molecular simulations, is 671 m^2/g. Owing to its simple, high-yield synthesis at low temperatures, porosity, and electrical conductivity, GTUB3 may be used as a low-cost electrode material in next generation phosphonate-supercapacitors.

Introduction

Metal-organic frameworks (MOFs) are microporous compounds that can reach very high surface areas of over 7000 m^2/g. [1-3] The majority of MOFs in the literature are synthesized using derivatives of arylcarboxylic acid linkers. [4-10] Traditional arylcarboxylate MOFs often contain well-defined molecular inorganic building units (IBUs) such as paddle wheel patterns. [6, 7] The ligand-binding modes around such molecular IBUs form large angles, ensuring separation between the organic struts and, in turn, resulting in large void spaces. [11] On the other hand, such separation limits the electrostatic interactions between the organic linkers. Therefore, traditional MOFs lack the required electron hopping and extended conjugation mechanisms between the bridging ligands to support electron mobility. [12-14] Although high surface area MOFs are ideal platforms to host electrons for supercapacitor applications, due to the lack of such mechanisms, conventional arylcarboxylate MOFs are generally known to be insulators.

Recently, two-dimensional π-stacked MOFs based on ortho-diimine, ortho-dihydroxy, azolate, and thiolate metal-binding groups have exhibited very high electrical conductivity. [12, 14-20] Due to the conservative, strongly chelating metal-binding modes of ortho-diimine and ortho-dihydroxy linkers, these systems are limited to the planar X- and Y-shaped linker geometries. Therefore, efforts to optimize the surface area and conductance in these systems has been rather limited. In a similar fashion, it has been very difficult to covalently modify graphene and activated carbon electrode materials to optimize their conductivities and surface areas. [21] MOFs with metal-binding groups that provide higher structural diversity are required to produce the next generation of electrode materials in supercapacitor applications, e.g., the use of supercapacitors to reduce the charging time in electrically powered vehicles.[22, 23] In this connection, phosphonates are the most structurally diverse metal-binding groups with three oxygens available for metal-binding in various coordination modes as shown in Harris notation.

A

[24-27] In addition, several phosphonate MOFs are known to exhibit exceptionally high thermal and chemical stabilities, which would be beneficial for their use in the presence of water, electrolytes, or even acids. [28-30] To the best of our knowledge, less than 0.003% of all known MOFs reported in the structural databases are phosphonate MOFs, which are constructed using aromatic phosphonic acid linkers. [25,31,32] Owing to the aforementioned advantages, phosphonate MOFs may allow for structural variations that generate high electrical conductivity and high surface areas for charge holding and be sufficiently stable for use in industrial applications.

Semiconductive Phosphonate MOFs

Recently, we reported the first highly stable semiconductive copper-phosphonate MOFs TUB75 and TUB40 with directionally dependent electrical conductivities in the 10^{-3} and 10^{3} S/m range. [33-35] In a related study, we reported the first semiconductive permanently microporous hydrogen-bonded phosphonic acid framework (constructed using the *p*-H_8TPPA linker) with a band gap of 1.54 eV. [36] To the best of our knowledge, no semiconductive zinc-phosphonate MOFs have been reported in the literature. Thus, in this work, we used the polyaromatic porphyrin core with zinc IBUs to synthesize a semiconductive zinc-phosphonate MOF known as GTUB3. To produce mono-deprotonated phosphonic acid metal-binding groups, we carried out a pH-controlled deprotonation of the Cu-*p*-H_8TPPA linker. [34] The four mono-deprotonated phosphonate groups in Cu-*p*-H_4TPPA^{-4} are involved in the formation of the tetrahedral zinc atoms. Each of the zinc atoms is coordinated to a mono-deprotonated phosphonic acid tether of Cu-*p*-H_4TPPA^{-4}, allowing us to achieve the simplest tetrahedral ZnO_4 metal-binding modes and thereby ensuring the extended conjugation of the porphyrin core throughout the MOF. This generates short π-stacking between the planar porphyrin units, which may also promote electron hopping. Together, these features result in a relatively high electrical conductivity of 4 S/m (see reference [14] for a comprehensive list of 3D MOFs and their

electrical conductivities). The low band gap of 1.64 eV points to the semiconducting nature of GTUB3.

Synthesis of GTUB3

Due to the rich metal-binding modes of arylphosphonic acids, M-O-M condensations result in unpredictable oligomerizations of metal-phosphonate polyhedra in one, two, and even in three dimensions. [37, 38] Therefore, to achieve predictable synthesis in metal phosphonate chemistry, it is important to restrain the metal-binding modes. Previously, we achieved the selective mono-deprotonation of arylphosphonic acid using a pH-controlled synthesis. We adapted the same strategy in this work to reproduce the simplest metal-binding modes observed previously in GTUB4. [34]

The Cu(*p*-H_8TPPA) linker (see Figure 1a) was synthesized according to our previously reported method (see Figure S3 for the synthetic pipeline). [34] The single crystals of GTUB3 were synthesized in scintillation vials after the reaction of 0.03 mmol $Zn(NO_3)_2 \cdot 6H_2O$, 0.01 mmol Cu-H_8TPPA, and 1.5 mmol phenylphosphonic acid at 80 °C in the presence of 10 ml:7.5 ml DMF/H_2O and pH values between 1.7 and 7 (to ensure the mono-deprotonation of the phosphonic acids). The yield of the reaction was 90% and the purity of the crystals was confirmed by EDX elemental analysis (see Figure S4).

Structure of GTUB3

One of the preferred coordination environments for a zinc atom is tetrahedral. Thus, it is expected that the square planar *p*-H_8TPPA linker will produce a 3D MOF structure when it coordinates to the tetrahedral zinc atom (following the simplest Harris notation). Figures 1a, b and c show the structure of GTUB3, which was solved using single-crystal X-ray diffraction (see SI for crystallographic refinement details and Tables S1 and S2 for bond distances). As

seen in Figure 1c, the selectively mono-deprotonated *p*-H_8TPPA linkers coordinate with the tetrahedral zinc atoms to generate a 3D structure. GTUB3 is unique compared to other 3D phosphonate metal-organic solids with tetrahedral molecular IBUs. It has a negatively charged framework of [Zn(Cu-*p*-H_4TPPA)]$^{-2}$ and the presence of two dimethylammonium cations in the pore sites provide charge balance. The presence of sp^2-bound phenylphosphonic acid around the porphyrin core results in extended conjugation throughout the 3D framework. Furthermore, as seen in Figure 1b, the highly conjugated planar tetratopic *p*-H_8TPPA linkers are separated by a distance of ca. 4.2 Å, which leads to electrostatic interactions between each of the porphyrin units and possibly electron hopping. Furthermore, the pyrrole ring of the *p*-H_8TPPA core has a square planar Cu(II) atom, which is known to provide high energy electrons. Finally, the textural properties of GTUB3 were calculated using the Poreblazer v4.0 software [31]. We obtained a N_2-accessible geometric surface area of 671 m^2/g, pore widths of 4 to 6 Å (Figure S6), and a helium-accessible pore volume of 0.43 cm^3/g.

Band Gap Measurement

We generated the Tauc plot of the solid-state diffuse reflectance spectrum (DRS) of hand-picked single crystals of GTUB3 to estimate its band gap (see Figure 2b). [39] From the Tauc plot, we see that GTUB3 has a low indirect band gap of 1.64 eV, characteristic of a semiconductor. The details of the DRS measurement and fitting may be found in the SI.

Electrical Conductivity Measurements

To measure the electrical conductivity of GTUB3, we developed a new technique that can quantify the average thickness of the crystals during impedance spectroscopy. This technique is especially useful when the crystal size is less than 1 mm^3 and the crystals are randomly oriented and not uniformly covering the surface, which is the case for GTUB3 (see Figure 2a). The details of the experimental setup may be found in the SI.

We used a two-electrode jig system made of mirror-polished and gold-coated copper discs of diameter 12.7 mm and height 6.35 mm. The electrodes were placed between the anvil and spindle of a standard micrometer, insulated by PLA (3D printer filament), and heat-treated for the optimal alignment of the electrodes. We recorded the impedance values (using the Digilent Analog Discovery 2 with impedance analyzer) before and after mounting the samples, for each electrode separation increment/decrement of 0.01mm, between 100Hz-1MHz (as seen in Figure 2c). We have estimated the parallel capacitance (which is ca. 8 pF) and offset distance of the electrodes at close proximity and compensated for these values in the measured values when the sample is mounted. The extrapolation of the Nyquist plots to the real axis gave a resistance of ~ 200 Ω (see Figure **2c**). Since the conductivity is given by $\sigma=L/RA$ (where L is the length of the sample, R is the resistance, and A is the contact surface area) and L=0.08mm and A=13mm^2 in our case (estimated from an optical microscope image), we find the minimum conductivity to be σ_{min}= 0.03 S/m. This value represents the lowest estimate of the electrical conductivity of the GTUB3 crystals, as the actual contact surface area is less than the total surface area of the crystals. Thus, the actual conductance is expected to be higher.

We also performed DC measurements under an optical microscope, by directly pressing on the crystals with a stainless-steel probe attached to a three-axis micromanupulator system connected to a Keithley DMM4050 digital multimeter. After compensating for the probe/wire resistance, we measured resistance values between 100Ω and 300Ω for different crystals and crystal orientations, in good agreement with the impedance measurements. The single-crystal surface area for this measurement is ca. 0.1 mm^2 (estimated from an optical microscope image)**.** Therefore, the DC measurements on single crystals yield a range of conductances between σ = 2 S/m and σ = 8 S/m (NB: σ = 4 S/m based on the average resistance of 200 Ω). The small

range of observed conductances suggests that the conductivity of GTUB3 is non-directional, which is likely due to the extended conjugation throughout the 3D GTUB3 crystal structure.

Thermal Properties

Thermogravimetric analysis (TGA) of GTUB3 shows a two-step weight loss of solvent molecules totaling 12.4 % until ca. 300 °C (see Figure S5). The sharp weight loss beginning at ca. 400 °C, as seen in the previously reported porphyrin-phosphonate MOFs, indicates the decomposition of the organic linker. The thermal decomposition of GTUB3 continues above 900 °C, which might be indicative of the formation of heat-stable organophosphide species between 400 and 450 °C. [40, 41] Therefore, it was not possible to compare the theoretical and calculated weight losses. This unusual decomposition pattern is unique to *p*-H_8TPPA and MOFs constructed using *p*-H_8TPPA. For example, similar TGA patterns have also been observed in the thermal decomposition profiles of the starting materials Cu(*p*-H_8TPPA) and *p*-H_8TPPA, and also GTUB4, a nanotubular [Ni(Cu-*p*-H_4TPPA)]·2 $(CH_3)_2NH_2^+$ MOF (for a comparison, see Figure S5). [34, 42]

Conclusions

Herein, we report the synthesis of GTUB3, a 3D zinc-phosphonate MOF. The electrical conductivity measurements indicate that it has a high, non-directional average electrical conductivity of 4 S/m, making GTUB3 the first conductive zinc-phosphonate MOF in the literature and a rare example of a conductive 3D zinc MOF. The sp^2-bonded phenylphosphonates ensure the extension of the conjugation of the porphyrin core into the 3D framework via the tetrahedral zinc ions, which we believe is why GTUB3 exhibits a non-directional conductivity. Presumably, polyaromatic phosphonic acid bridging ligands with tetrahedral zinc IBUs may also produce electrically conductive MOFs. We are currently working on expanding our conductive zinc MOF library using different linker geometries. Due

to its porosity, non-directional conductivity, high-yield synthesis, and low cost, GTUB3 may be used as an electrode material for supercapacitors.

Author contributions

Gündoğ Yücesan created the hypothesis, supervised the project, and wrote the manuscript. Yunus Zorlu synthesized the compound, solved the structure using single-crystal X-ray diffraction, and performed the TGA. Patrik Tholen contributed to the crystal structure refinement. A. Ozgur Yazaydin carried out the molecular simulations of the textural and wrote the related text. M. Menaf Ayhan generated the Tauc plot of the DRS spectrum. Ozgur Yavuzcetin took the scanning electron microscope images, designed and constructed the new equipment for measuring the electrical conductivity, measured the conductance, and wrote the corresponding sections in the manuscript. Gabriel Hanna performed extensive critical revisions of the entire manuscript and edited the entire manuscript.

Funding

Gündoğ Yücesan would like to thank the DFG for funding his work. A. Ozgur Yazaydin acknowledges the German Academic Exchange Service (DAAD) for funding his visit to TU-Berlin (grant number 57507438).

Competing interests

Authors declare no competing interests. Gündoğ Yücesan has a patent pending for some of the presented results.

Data and materials availability

All data and details of the synthesis, EDS spectra, electrical conductivity and DC measurements, molecular simulations, X-ray refinement, and band gap measurement are available in the main text and Supplementary Information. The X-ray crystallographic coordinates for the structure reported in this study can be obtained free of charge from the Cambridge Crystallographic Data Centre (CCDC) [under the deposition number CCDC: 2052211 for GTUB3] via www.ccdc.cam.ac.uk/data_request/cif.

References

1. Farha, O. K.; Eryazici, I.; Jeong, N. C.; Hauser, B. G.; Wilmer, C. E.; Sarjeant, A. A.; Snurr, R. Q.; Nguyen, S. T.; Yazaydın, A.; Hupp, J. T., Metal-organic framework materials with ultrahigh surface areas: is the sky the limit? *J Am Chem Soc* **2012,** *134* (36), 15016-21.

2. Grünker, R.; Bon, V.; Müller, P.; Stoeck, U.; Krause, S.; Mueller, U.; Senkovska, I.; Kaskel, S., A new metal-organic framework with ultra-high surface area. *Chem Commun (Camb)* **2014,** *50* (26), 3450-2.

3. Hönicke, I. M.; Senkovska, I.; Bon, V.; Baburin, I. A.; Bönisch, N.; Raschke, S.; Evans, J. D.; Kaskel, S., Balancing Mechanical Stability and Ultrahigh Porosity in Crystalline Framework Materials. *Angew Chem Int Ed Engl* **2018,** *57* (42), 13780-13783.

4. Evans, J. D.; Garai, B.; Reinsch, H.; Li, W.; Dissegna, S.; Bon, V.; Senkovska, I.; Fischer, R. A.; Kaskel, S.; Janiak, C.; Stock, N.; Volkmer, D., Metal–organic frameworks in Germany: From synthesis to function. *Coordination Chemistry Reviews* **2019,** *380*, 378-418.

5. Zhou, H. C.; Long, J. R.; Yaghi, O. M., Introduction to metal-organic frameworks. *Chem Rev* **2012,** *112* (2), 673-4.

6. Yaghi, O. M.; O'Keeffe, M.; Ockwig, N. W.; Chae, H. K.; Eddaoudi, M.; Kim, J., Reticular synthesis and the design of new materials. *Nature* **2003,** *423* (6941), 705-14.

7. Kalmutzki, M. J.; Hanikel, N.; Yaghi, O. M., Secondary building units as the turning point in the development of the reticular chemistry of MOFs. *Sci Adv* **2018,** *4* (10), eaat9180.

8. Yuan, S.; Feng, L.; Wang, K.; Pang, J.; Bosch, M.; Lollar, C.; Sun, Y.; Qin, J.; Yang, X.; Zhang, P.; Wang, Q.; Zou, L.; Zhang, Y.; Zhang, L.; Fang, Y.; Li, J.; Zhou, H.-C., Stable Metal–Organic Frameworks: Design, Synthesis, and Applications. *Advanced Materials* **2018,** *30* (37), 1704303.

9. Li, H.; Eddaoudi, M.; O'Keeffe, M.; Yaghi, O. M., Design and synthesis of an exceptionally stable and highly porous metal-organic framework. *Nature* **1999,** *402* (6759), 276-279.

10. Schneemann, A.; Bon, V.; Schwedler, I.; Senkovska, I.; Kaskel, S.; Fischer, R. A., Flexible metal-organic frameworks. *Chem Soc Rev* **2014,** *43* (16), 6062-96.

11. Deng, H.; Grunder, S.; Cordova, K. E.; Valente, C.; Furukawa, H.; Hmadeh, M.; Gándara, F.; Whalley, A. C.; Liu, Z.; Asahina, S.; Kazumori, H.; O'Keeffe, M.; Terasaki, O.; Stoddart, J. F.; Yaghi, O. M., Large-Pore Apertures in a Series of Metal-Organic Frameworks. *Science* **2012,** *336* (6084), 1018.

12. Sun, L.; Campbell, M. G.; Dincă, M., Electrically Conductive Porous Metal–Organic Frameworks. *Angew. Chem., Int. Ed.* **2016,** *55*, 3566.

13. Skorupskii, G.; Trump, B. A.; Kasel, T. W.; Brown, C. M.; Hendon, C. H.; Dincă, M., Efficient and Tunable One-Dimensional Charge Transport in Layered Lanthanide Metal-Organic Frameworks. *Nat. Chem.* **2020,** *12*, 131.

14. Xie, L. S.; Skorupskii, G.; Dincă, M., Electrically Conductive Metal–Organic Frameworks. *Chemical Reviews* **2020,** *120* (16), 8536-8580.

15. Xie, L. S.; Alexandrov, E. V.; Skorupskii, G.; Proserpio, D. M.; Dincă, M., Diverse π–π Stacking Motifs Modulate Electrical Conductivity in Tetrathiafulvalene-Based Metal–Organic Frameworks. *Chem. Sci.* **2019,** *10*, 8558.

16. Sheberla, D.; Bachman, J. C.; Elias, J. S.; Sun, C. J.; Shao-Horn, Y.; Dinca, M., Conductive MOF Electrodes for Stable Supercapacitors with High Areal Capacitance. *Nat. Mater.* **2017,** *16*, 220.

17. Dou, J.-H.; Arguilla, M. Q.; Luo, Y.; Li, J.; Zhang, W.; Sun, L.; Mancuso, J. L.; Yang, L.; Chen, T.; Parent, L. R.; Skorupskii, G.; Libretto, N. J.; Sun, C.; Yang, M. C.; Dip, P. V.; Brignole, E. J.; Miller, J. T.; Kong, J.; Hendon, C. H.; Sun, J.; Dincă, M., Atomically precise single-crystal structures of electrically conducting 2D metal–organic frameworks. *Nature Materials* **2020**.

18. Dong, R.; Zhang, Z.; Tranca, D. C.; Zhou, S.; Wang, M.; Adler, P.; Liao, Z.; Liu, F.; Sun, Y.; Shi, W., A Coronene-Based Semiconducting Two-Dimensional Metal-Organic Framework with Ferromagnetic Behavior. *Nat. Commun.* **2018,** *9*, 2637.

19. Nam, K. W.; Park, S. S.; dos Reis, R.; Dravid, V. P.; Kim, H.; Mirkin, C. A.; Stoddart, J. F., Conductive 2D Metal-Organic Framework for High-Performance Cathodes in Aqueous Rechargeable Zinc Batteries. *Nat. Commun.* **2019,** *10*, 4948.

20. Huang, X.; Yao, H.; Cui, Y.; Hao, W.; Zhu, J.; Xu, W.; Zhu, D., Conductive Copper Benzenehexathiol Coordination Polymer as a Hydrogen Evolution Catalyst. *ACS Applied Materials & Interfaces* **2017,** *9* (46), 40752-40759.

21. Clancy, A. J.; Au, H.; Rubio, N.; Coulter, G. O.; Shaffer, M. S. P., Understanding and controlling the covalent functionalisation of graphene. *Dalton Trans* **2020,** *49* (30), 10308-10318.

22. Li, W. H.; Ding, K.; Tian, H. R.; Yao, M. S.; Nath, B.; Deng, W. H.; Wang, Y.; Xu, G., Conductive Metal-Organic Framework Nanowire Array Electrodes for High-Performance Solid-State Supercapacitors. *Adv. Funct. Mater.* **2017,** *27*, 1702067.

23. Liu, J.; Song, X.; Zhang, T.; Liu, S.; Wen, H.; Chen, L., 2D Conductive Metal-Organic Frameworks: An Emerging Platform for Electrochemical Energy Storage. *Angew Chem Int Ed Engl* **2020**.

24. Coxall, R. A.; Harris, S. G.; Henderson, D. K.; Parsons, S.; Tasker, P. A.; Winpenny, R. E. P., Inter-ligand reactions: in situ formation of new polydentate ligands. *Journal of the Chemical Society, Dalton Transactions* **2000,** (14), 2349-2356.

25. Yücesan, G.; Zorlu, Y.; Stricker, M.; Beckmann, J., Metal-organic solids derived from arylphosphonic acids. *Coordination Chemistry Reviews* **2018,** *369*, 105-122.

26. Shearan, S. J. I.; Stock, N.; Emmerling, F.; Demel, J.; Wright, P. A.; Demadis, K. D.; Vassaki, M.; Costantino, F.; Vivani, R.; Sallard, S.; Ruiz Salcedo, I.; Cabeza, A.; Taddei, M., New Directions in Metal Phosphonate and Phosphinate Chemistry. *Crystals* **2019,** *9* (5).

27. Gagnon, K. J.; Perry, H. P.; Clearfield, A., Conventional and unconventional metal-organic frameworks based on phosphonate ligands: MOFs and UMOFs. *Chem Rev* **2012,** *112* (2), 1034-54.

28. Gao, C. Y.; Ai, J.; Tian, H. R.; Wu, D.; Sun, Z. M., An ultrastable zirconium-phosphonate framework as bifunctional catalyst for highly active CO. *Chem Commun (Camb)* **2017,** *53* (7), 1293-1296.

29. Zheng, T.; Yang, Z.; Gui, D.; Liu, Z.; Wang, X.; Dai, X.; Liu, S.; Zhang, L.; Gao, Y.; Chen, L.; Sheng, D.; Wang, Y.; Diwu, J.; Wang, J.; Zhou, R.; Chai, Z.; Albrecht-Schmitt, T. E.; Wang, S., Overcoming the crystallization and designability issues in the ultrastable zirconium phosphonate framework system. *Nat Commun* **2017,** *8*, 15369.

30. Zorlu, Y.; Erbahar, D.; Çetinkaya, A.; Bulut, A.; Erkal, T. S.; Yazaydin, A. O.; Beckmann, J.; Yücesan, G., A cobalt arylphosphonate MOF - superior stability, sorption and magnetism. *Chem Commun (Camb)* **2019,** *55* (21), 3053-3056.

31. Sarkisov, L.; Bueno-Perez, R.; Sutharson, M.; Fairen-Jimenez, D., Materials Informatics with PoreBlazer v4.0 and the CSD MOF Database. *Chemistry of Materials* **2020,** *32* (23), 9849-9867.

32. Wilmer, C. E.; Leaf, M.; Lee, C. Y.; Farha, O. K.; Hauser, B. G.; Hupp, J. T.; Snurr, R. Q., Large-scale screening of hypothetical metal–organic frameworks. *Nat. Chem.* **2012,** *4* (2), 83.

33. Siemensmeyer, K.; Peeples, C. A.; Tholen, P.; Schmitt, F. J.; Çoşut, B.; Hanna, G.; Yücesan, G., Phosphonate Metal-Organic Frameworks: A Novel Family of Semiconductors. *Adv Mater* **2020,** *32* (24), e2000474.

34. Ayhan, M. M.; Bayraktar, C.; Yu, K. B.; Hanna, G.; Yazaydin, A. O.; Zorlu, Y.; Yücesan, G., A Nanotubular Metal-Organic Framework with a Narrow Bandgap from Extended Conjugation*. *Chemistry* **2020,** *26* (65), 14813-14816.

35. Peeples, C. A.; Kober, D.; Schmitt, F.-J.; Tholen, P.; Siemensmeyer, K.; Halldorson, Q.; Çoşut, B.; Gurlo, A.; Yazaydin, A. O.; Hanna, G.; Yücesan, G., A 3D Cu-Naphthalene-Phosphonate Metal–Organic Framework with Ultra-High Electrical Conductivity. *Advanced Functional Materials* **2020**, 2007294.

36. Tholen, P.; Peeples, C. A.; Schaper, R.; Bayraktar, C.; Erkal, T. S.; Ayhan, M. M.; Çoşut, B.; Beckmann, J.; Yazaydin, A. O.; Wark, M.; Hanna, G.; Zorlu, Y.; Yücesan, G., Semiconductive microporous hydrogen-bonded organophosphonic acid frameworks. *Nat Commun* **2020,** *11* (1), 3180.

37. Bulut, A.; Wörle, M.; Zorlu, Y.; Kirpi, E.; Kurt, H.; Zubieta, J.; Grabowsky, S.; Beckmann, J.; Yücesan, G., A potential Cu/V-organophosphonate platform for tailored void spaces via terpyridine mold casting. *Acta Crystallogr B Struct Sci Cryst Eng Mater* **2017,** *73* (Pt 2), 296-303.

38. Cao, G.; Hong, H. G.; Mallouk, T. E., Layered metal phosphates and phosphonates: from crystals to monolayers. *Accounts of Chemical Research* **1992,** *25* (9), 420-427.

39. Tauc, J.; Grigorovici, R.; Vancu, A., Optical Properties and Electronic Structure of Amorphous Germanium. *physica status solidi (b)* **1966,** *15* (2), 627-637.

40. Yi, T.; Zhang, G.; Tsujii, N.; Fleurial, J.-P.; Zevalkink, A.; Snyder, G. J.; Grønbech-Jensen, N.; Kauzlarich, S. M., Phase Characterization, Thermal Stability, High-Temperature Transport Properties, and Electronic Structure of Rare-Earth Zintl Phosphides Eu3M2P4 (M = Ga, In). *Inorganic Chemistry* **2013,** *52* (7), 3787-3794.

41. Zhang, R.; Russo, P. A.; Feist, M.; Amsalem, P.; Koch, N.; Pinna, N., Synthesis of Nickel Phosphide Electrocatalysts from Hybrid Metal Phosphonates. *ACS Applied Materials & Interfaces* **2017,** *9* (16), 14013-14022.

42. Enakieva, Y. Y.; Sinelshchikova, A. A.; Grigoriev, M. S.; Chernyshev, V. V.; Kovalenko, K. A.; Stenina, I. A.; Yaroslavtsev, A. B.; Gorbunova, Y. G.; Tsivadze, A. Y., Highly Proton-Conductive Zinc Metal-Organic Framework Based On Nickel(II) Porphyrinylphosphonate. *Chemistry – A European Journal* **2019,** *25* (45), 10552-10556.

Experimental Section

CCDC 2052211 contains the supplementary crystallographic data for this paper. This data can be obtained free of charge from The Cambridge Crystallographic Data Centre via www.ccdc.cam.ac.uk/data_request/cif.

Acknowledgements

Gündoğ Yücesan would like to thank the DFG for funding his work. A. Ozgur Yazaydin would like to thank DAAD for supporting his visit to TU-Berlin.

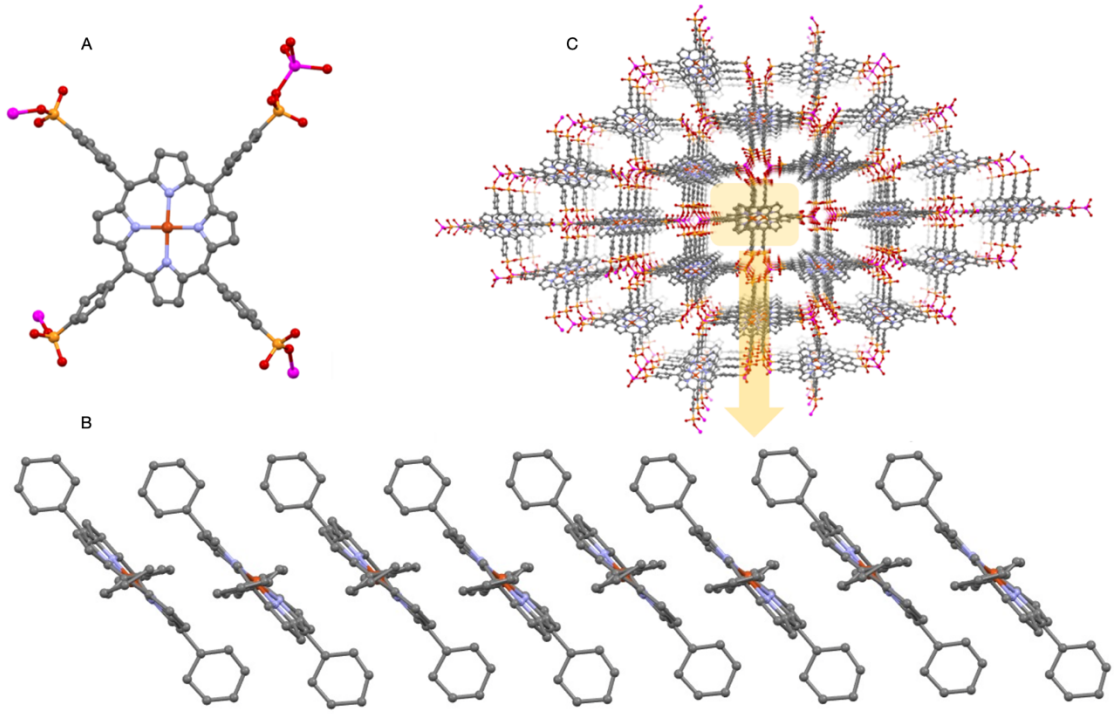

Figure 1. a) Crystal structure of Cu-H_8TPPA and the zinc coordination modes around the phosphonic acids. b) Domino-like packing of the porphyrin units in GTUB3, which are separated by a distance of 4.2 Å. c) 3D structure and view of pores in GTUB3.

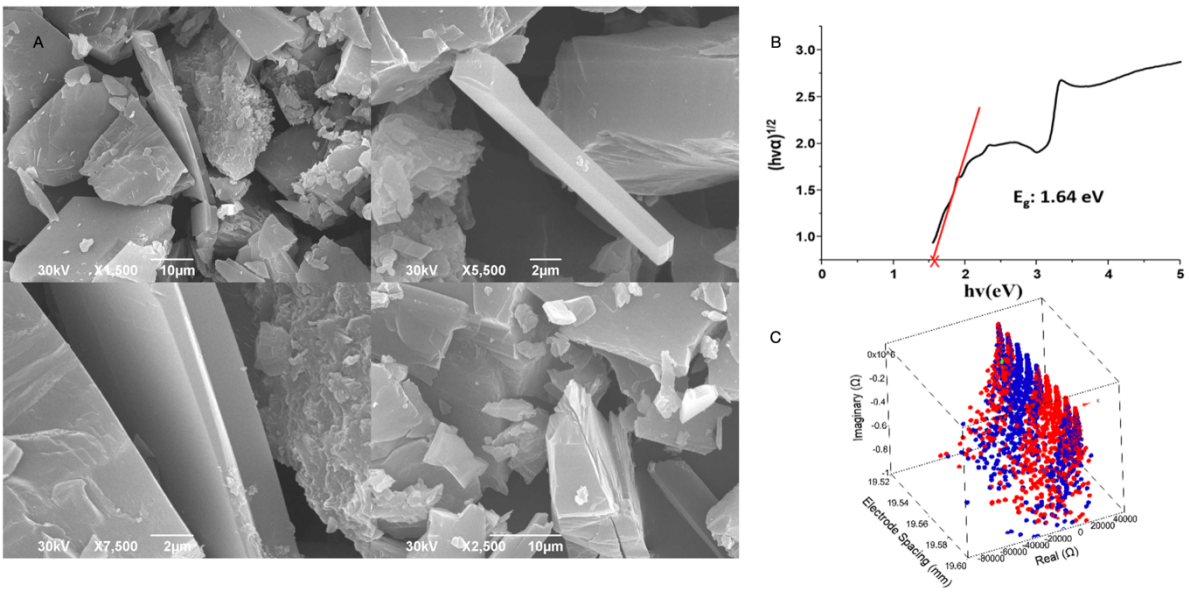

Figure 2. a) SEM pictures of GTUB3 crystals non-uniformly arranged on a surface with random orientations. b) Tauc plot of the diffuse reflectance spectrum of GTUB3, showing an estimate of the indirect band gap. c) Real and imaginary Nyquist plots of impedance sweeps as

a function of electrode spacing (non-offset values). The red and blue dots represent the Nyquist plots for each increment/decrement in electrode gap distance.